

Functionalization with polymer ligands enhances the catalytic activity of surfactant-stabilized gold nanoparticles

Supporting Information

Sophie Jancke^{1,2} and Christian Rossner*^{1,2,3}

¹Leibniz-Institut für Polymerforschung Dresden e.V., D-01069 Dresden, Germany.

²Faculty of Chemistry and Food Chemistry, Technische Universität Dresden, D-01069 Dresden, Germany.

³Department of Polymers, University Chemistry and Technology Prague, Technická 5, Prague 6 16628, Czech Republic.

E-mail: rossner@ipfdd.de

Table of contents

1. Literature comparison table
2. Experimental conditions for CTAC@AuNP synthesis
3. SEC results of PDMAM polymers
4. Comparison of our functionalization approach (standard) to 2-phase CTAC extraction
5. Characterization results for nanoparticles before and after functionalization with polymer ligands
6. Catalysis test conditions, calculation to keep total gold surface constant and kinetic fit
7. Characterization of substrate-deposited samples for heterogeneous catalysis
8. Fitting light response data using modified Mitscherlich model
9. Calculation of plasmonic heating
10. Literature

1) Literature comparison table

Table S1: Comparison of publications on catalysis in solution from ex-situ synthesized Au nanoparticles: catalytic performance with different ligands vs. particles as synthesized.

Ligand	NPs as synthesized	Ligand	Reaction	Ligand effect	Reference
Relative Catalytic Activity					
	CTAC@AuNPs	PDMAM-RAFT 4.5 kDa 49 kDa	H ₂ O ₂ -mediated MB decomposition	Increased activity, dependent on M _n	This work
PEG-SH 1 kDa ←····· 30 kDa	citrate@AuNPs		BH ₄ -Reduction of 4-Nitrophenol	Activity dependent on M _n	Ansar 2016 ¹
PEG-SH PEG-NH	citrate@AuNPs		BH ₄ -Reduction of: - 4-Nitrophenol - Rhodamine B - Methylene Blue	Activity dependent on binding moiety	Piella 2017 ²
PS-SH	citrate@AuNPs	PS-NHC	BH ₄ -Reduction of 4-Nitrophenol	Increased/ reduced activity dependent on binding moiety	Zhang 2020 ³
PS-PNIPA @45°C @23°C	citrate@AuNPs		BH ₄ -Reduction of Fe(CN) ₆ ⁻³	Activity change via temperature	Hervéz 2012 ⁴
PEG-SH 2 kDa 0.4 kDa	citrate@AuNPs		BH ₄ -Reduction of 4-Nitrophenol	Activity dependent on binding moiety	Ciganda 2014 ⁵
PVP 50 mM ←····· 12 mM	citrate@AuNP		BH ₄ -Reduction of 4-Nitrophenol	Activity dependent on concentration	Alvarez- Cerimendo 2019 ⁶
PAA-SH 50% SH ←····· 10% SH 2 kDa 30 kDa	citrate@AuNP		BH ₄ -Reduction of 4-Nitrophenol	Catalyst recovery via Agglomeration by pH Activity dependent on thiol content, M _n	Chakraborty 2019 ⁷

2) Experimental Conditions for CTAC@AuNP Synthesis

Table S2: Synthesis conditions, including volumes and concentrations, to obtain differently sized spherical CTAC@AuNPs.

		CTAB	HAuCl ₄	NaBH ₄
1	<i>c</i>	0.1 M	100 mM	10 mM
	<i>V</i>	4.7 mL	12.5 μL	300 μL
	<i>n</i>	0.47 mmol	1.25 μmol	3 μmol
	eq.		1	2.4
		CTAC	HAuCl ₄	AsCH ₂
2	<i>c</i>	200 mM	0.5 mM	100 mM
	<i>V</i>	40 mL	40 mL	30 mL
	<i>n</i>	8 mmol	0.02 mmol	3 mmol
	eq.	400	1	150
3	<i>c</i>	60 mM	1 mM	100 mM
	<i>V</i>	200 mL (2x)	200 mL	2.6 mL
	<i>n</i>	12 mmol	0.2 mmol	260 μmol
	eq.	6	1	0.13

+ different volumes of seed solution depending on NP size as listed below

Nanoparticle Diameter [nm]	Volume Seed solution (from 2, 20 mL)
28	20 mL
34	4 mL
43	2 mL
45	2 mL
57	1 mL

3) SEC Data Polymer

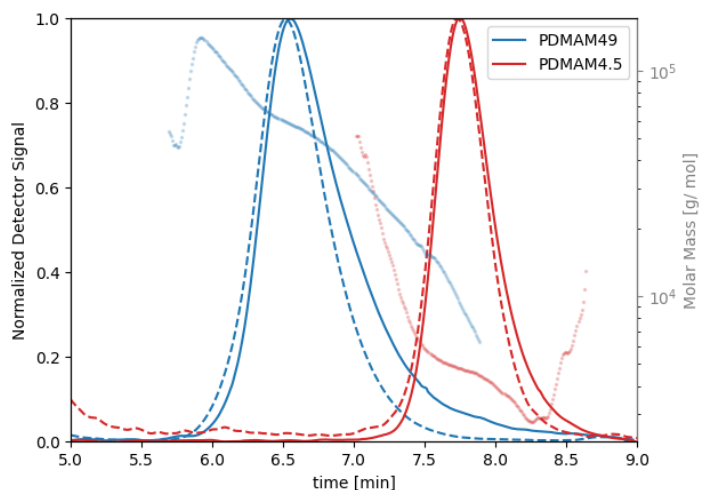


Figure S1. Result of size exclusion chromatography for PDMAM4.5 and PDMAM49: Solid line from refractive index detector, dashed line from light-scattering detector.

4) Comparison of our functionalization approach (standard) to 2-phase CTAC extraction

Table S3: Conditions for ligand exchange. An Elmasonic P bath was used for sonication.

		Nanoparticle Solution (from 3)
Centrifugation	V	1 mL
	Speed	3.0 krcf
	Time	20 min
	N (centrifugation)	3x (28); 2x (34, 43, 45, 57 nm)
		Polymer (PDMAM 4.5 kDa)
Functionalization	m	2 mg
	Time (ultrasound)	5 min @37 kHz
	Time (incubation)	>12 h
		Polymer (PDMAM 49 kDa)
Functionalization	m	5 mg
	Time (ultrasound)	5 min @37 kHz
	Time (incubation)	>12 h

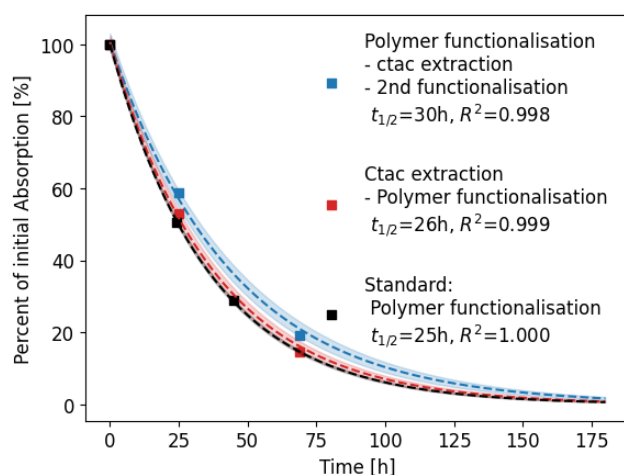


Figure S2. Methylene blue decomposition reaction with first order fit for catalyst produced via 2-phase CTAC extraction and catalyst from centrifugation (n-1) method.

Figure S2 displays MB decomposition data obtained with differently produced PDMAM@AuNP catalyst. The black curve corresponds to the “standard” procedure for ligand exchange (n-1 method). The red curve was obtained by using CTAC extraction with chloroform before adding the polymer ligand according to Schulz et al. For the sample that resulted in the blue curve, first polymer was added, then a CTAC extraction step was performed followed by a second polymer functionalization step. As can be seen, no significant difference in catalytic performance was achieved.

5) Nanoparticle characterization before and after functionalization with polymer ligands

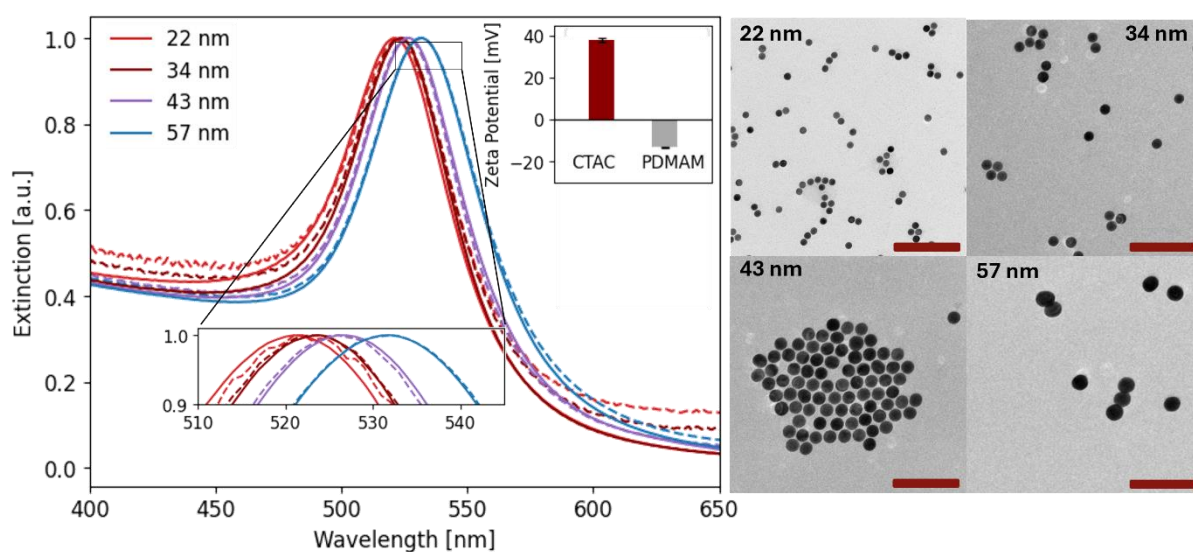


Figure S3. Left: Extinction spectra of differently sized AuNPs. Solid lines for CTAC-stabilized particles after synthesis. Dashed lines for PDMAM-stabilized particles. Inlet: Zeta potential before and after ligand exchange. Right: TEM images of CTAC-stabilized particles. Scale bar = 200 nm.

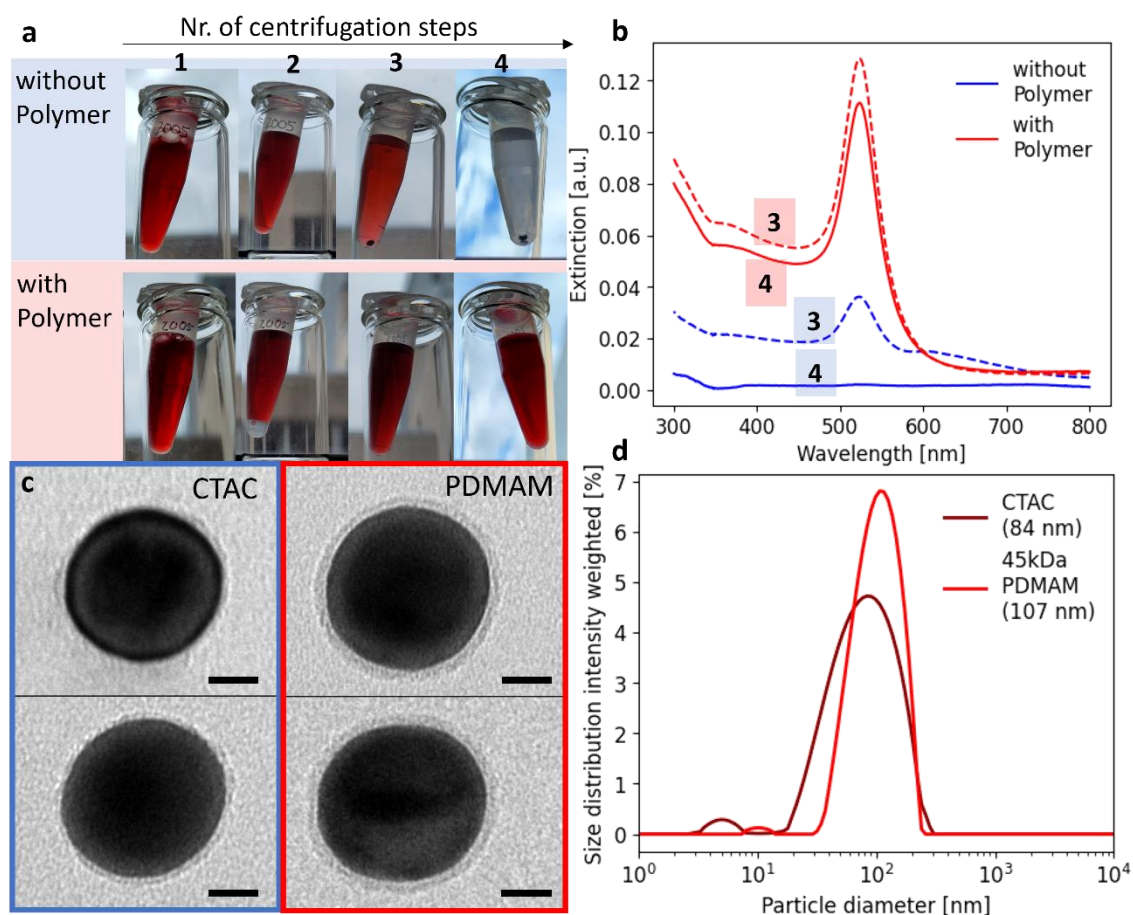


Figure S4 a: Comparison of ligand exchange process with vs. without adding polymer with image taken after each centrifugation step. b: Absorption spectra taken after the last two centrifugation steps (corresponding to images 3 and 4 in A. c: TEM image of two CTAC-stabilized particles vs. two polymer-functionalized particles from the same batch (scale bar = 2 nm) d: Intensity distribution from DLS as a measure of hydrodynamic diameter before and after functionalization. The values given in the legend correspond to the peak maxima.

6) Catalysis test conditions, calculation to keep total gold surface constant and kinetic fit

Table S4: Volumes and concentrations for catalysis experiments. Including three exemplaric hybrid gold solutions to illustrate how the surface area was kept constant in all catalytic reaction experiments.

	MB	H₂O₂	Solvent (-mixture)
<i>c</i>	1.56 mol	30%	
<i>V</i>	100 μL	50 μL	(1.85 - V _{AuNP}) mL
<i>n</i>	0.16 mmol	0.75 mmol	
eq.	1	4.69	
	PDMAM49@Au28	PDMAM49@Au34	PDMAM49@Au43
<i>V</i>	100 μL	100.4 μL	115.4 μL
Total surface area	3.03E+14 nm ²	3.03E+14 nm ²	3.03E+14 nm ²

Method for calculation of Au atom concentration from extinction spectrum and estimation of total surface area:⁸

$$c_{\text{Au}}[\text{mM}] = \frac{\text{Extinction @400 nm measured}}{1.2 (\text{Extinction @400 nm Literature})} * 0.5 (\text{Conc. Literature})$$

With the knowledge of the diameter from TEM and the gold-atom concentration, the number of particles in the solution and total surface area is calculated, assuming perfect spheres.

Kinetic fit for MB decomposition:

The maxima of MB absorption were recorded using extinction spectroscopy. They were plotted in percent of initial absorption vs. reaction time. Test-wise, zero, first and second order kinetics were fit to the data and the quality of the fit compared by the R² value. In this comparison, all room-temperature reactions were found to correspond best to a first order fit. The reaction kinetic at elevated temperatures was best described by zero order reaction kinetics. The formulas for zero, first and second order kinetics were defined according to the known rate laws as follows:⁹

$$\text{Zero order: } c = -k \cdot t + c_0$$

$$\text{First order: } c = c_0 \cdot \exp(-kt)$$

$$\text{Second order: } c = \frac{1}{c_0^{-1} + k \cdot t}$$

Here *t* is the time, *c* corresponds to the concentration and *c*₀ is a factor that was only explicitly given for the zero-order fit. For the other two, *c*₀ was a factor to be estimated by the fitting method. The (apparent) reaction rate coefficient *k* is used to compare different samples (of the same reaction order) to each other. When half-life time is given (for first order reaction only) this is equal to ln(2)/*k*. The fit was obtained using Scipy python package by the method of non-linear least squares (https://docs.scipy.org/doc/scipy/reference/generated/scipy.optimize.curve_fit.html).

7) Characterization of substrate-deposited samples for heterogeneous catalysis

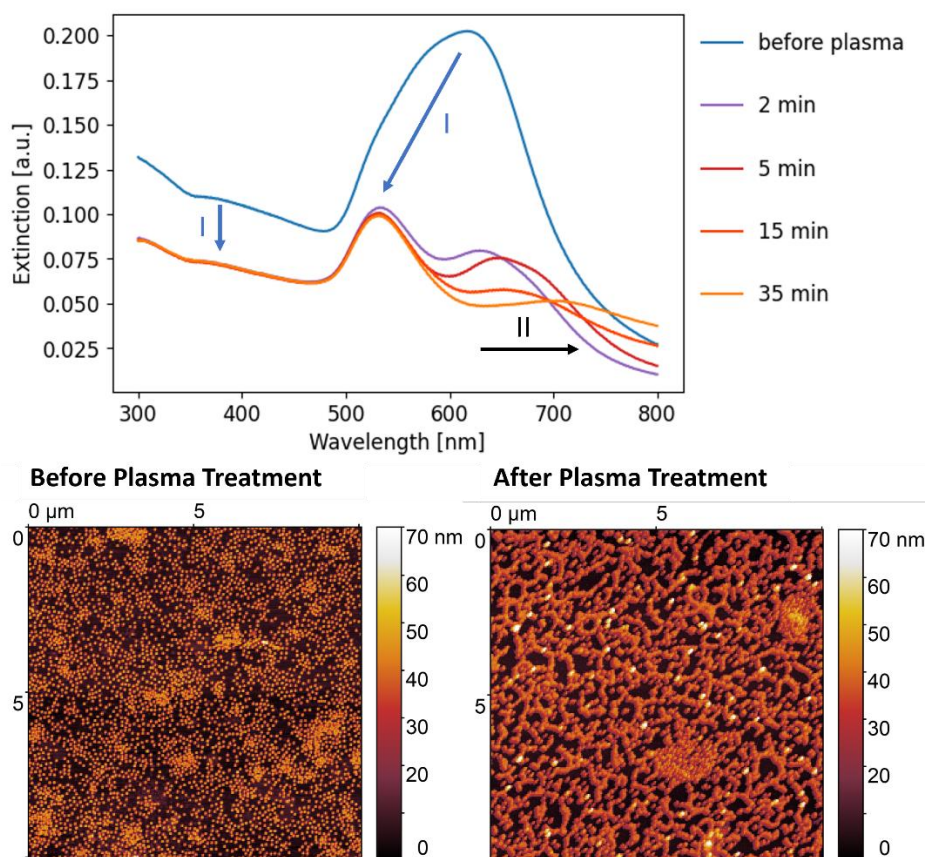


Figure S5 Upper panel: changes in the extinction spectrum of substrate-deposited Polymer@AuNPs after different plasma treatment times. Lower panel: comparison of AFM images of two samples, without (left) and with (right) plasma treatment.

Figure S5 (upper panel) shows the change in extinction spectra after different plasma treatment times. After two minutes pronounced changes are observed (I): A shift over the entire wavelength range towards lower extinction values is visible. Additionally, the plasmon peak splits and a separated red-shifted peak appears, indicating the presence of agglomerates. With longer treatment time, no further loss in extinction (especially visible in the high-energy region of the spectrum) is observed. The initial drop of extinction values is indicative of the loss of the polymer layer, which leads to a loss of two interfaces that give rise to scattering: the air-polymer and polymer-gold interface, which is not compensated by the emergence of the newly formed air-gold interface. This process appears to be already fully completed after two minutes. Afterwards, only a further redshift of the coupled plasmon peak can be observed (II), indicating further agglomerate growth and formation.

In the lower panel, for comparison AFM images of two samples are shown. The left was freshly prepared and not plasma treated. The one on the right underwent 10 minutes of plasma treatment. The difference is very clear: while in the left image, some areas appear slightly aggregated, the majority of the particles are individually scattered across the substrate. In the image on the right, network-like aggregates dominate with less single particles in between.

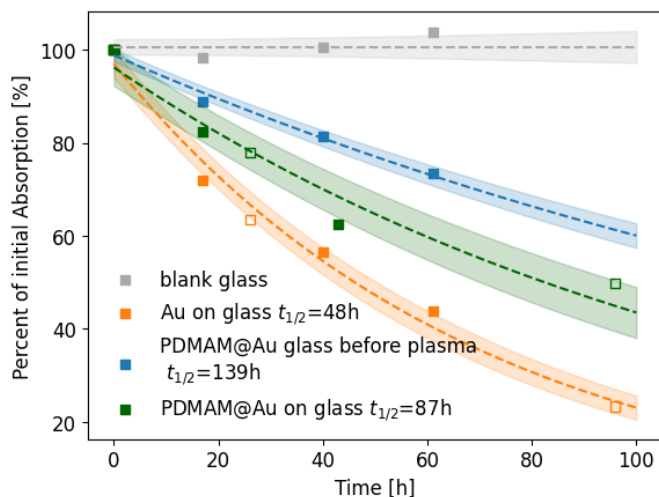


Figure S6 Comparison of catalytic activity of all substrate-deposited samples used in heterogenous catalysis. Blue corresponds to the PDMAM49@AuNP43 as deposited, orange to a sample that underwent plasma treatment and green to a sample re-functionalized with PDMAM49 polymer.

When comparing all three types of substrate-deposited samples, the as-deposited sample (blue) shows the lowest catalytic activity. There might be multiple explanations for this, but one difference before and after the plasma treatment is the presence of agglomerates, which may affect catalytic activity.

8) Fitting Light response data using modified Mitscherlich model

General form:

$$Y = A(1 - e^{-c(x+d)})$$

For photosynthesis following Liu et al. 2020:¹⁰

A = max rate, c = apparent quantum yield = slope of curve at low light level, x = PPF (photon flux), $-d$ = LCP = x -intercept (light compensation point) OPTIONAL: dark reaction R_d

$$Y = A_{max}(1 - e^{\frac{-Q(x-LCP)}{A_{max}}}) - R_d$$

9) Calculation of Plasmonic Heating

Absorption Cross sections of the particles were estimated following Mie theory using the Python package *miepython*¹¹ and refractive index values from Christy and Johnson.¹² Table S5 shows the estimated absorption cross section values at 496 nm and Figure S7 shows absorption and scattering cross section depending on wavelength.

Table S5 Absorption cross sections at 496 nm for differently sized gold nanoparticles, obtained from Mie Theory.

Size NP [nm]	Abs. Cross Section [nm ²]
22	171
43	1368
57	3356

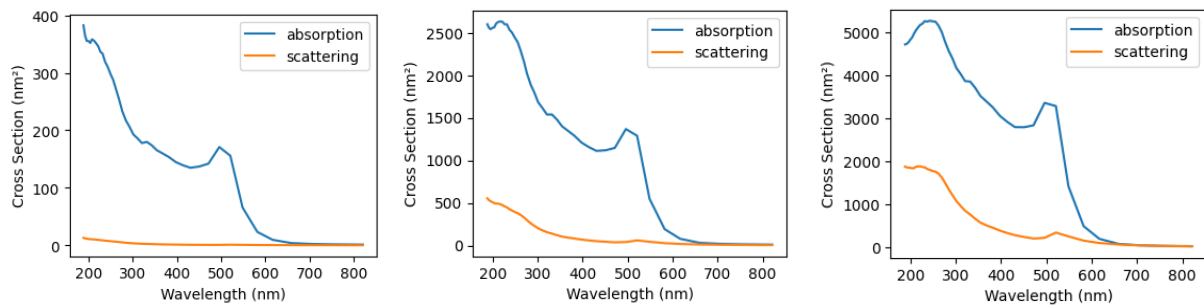


Figure S7 Theoretical absorption and scattering cross section vs. wavelength for differently sized gold nanoparticles obtained from Mie Theory using Christy and Johnson refractive index values.

The values are consistent in order of magnitude with an approximation given by Metwally *et al.* of $0.43 \times r^3 \text{ nm}^2$ for $r < 30$ and 532 nm .¹³

As stated by Alrahili *et al.* and Baffou *et al.* the temperature increase around a spherical particle in uniform medium can be described as

$$\Delta T = \frac{Q}{4\pi k_m r} = \frac{\sigma_{\text{abs}} I}{4\pi k_m r} \quad \text{for } r \geq R_{\text{NP}},$$

when steady state ($dT/dt=0$) is assumed.^{14,15}

The absorbed power Q can be obtained by multiplying the absorption cross section with the incoming power density. The latter was measured directly using a power meter and the obtained temperature profiles are shown in figure S8.

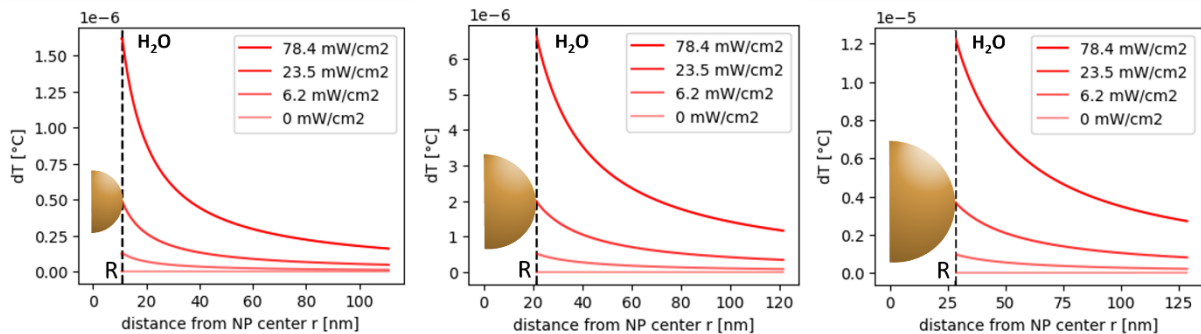


Figure S8 Theoretically estimated temperature changes in the solution surrounding the plasmonic particles, expected from plasmonic heating in the experimental setup used in this work.

Even for the biggest particles and highest measured light intensity the temperature increase is orders of magnitude away from any significant, measurable effect. The reason is the very small power density that arises from using an unfocussed light source. Comparable experiments in the literature used laser illumination with typical power densities between 10^3 and 10^6 W/cm².¹⁶ A given estimation of 38.8 K per mW/μm² from Chen et al. confirms our calculation: Again temperature changes in the order of 10⁻⁶ K are estimated when applied to our experimental setup.¹⁷

10) Literature

- 1 S. M. Ansar and C. L. Kitchens, *ACS Catal.*, 2016, **6**, 5553–5560.
- 2 J. Piella, F. Merkoçi, A. Genç, J. Arbiol, N. G. Bastús and V. Puntes, *J. Mater. Chem. A*, 2017, **5**, 11917–11929.
- 3 L. Zhang, Z. Wei, M. Meng, G. Ung and J. He, *J. Mater. Chem. A*, 2020, **8**, 15900–15908.
- 4 P. Hervés, M. Pérez-Lorenzo, L. M. Liz-Marzán, J. Dzubiella, Y. Lu and M. Ballauff, *Chem. Soc. Rev.*, 2012, **41**, 5577–5587.
- 5 R. Ciganda, N. Li, C. Deraedt, S. Gatard, P. Zhao, L. Salmon, R. Hernández, J. Ruiz and D. Astruc, *Chem. Commun.*, 2014, **50**, 10126–10129.
- 6 M. S. Álvarez Cerimedo, L. G. Baronio, C. E. Hoppe and M. A. Ayude, *ChemistrySelect*, 2019, **4**, 608–616.
- 7 S. Chakraborty and C. L. Kitchens, *J. Phys. Chem. C*, 2019, **123**, 26450–26459.
- 8 L. Scarabelli, A. Sánchez-Iglesias, J. Pérez-Juste and L. M. Liz-Marzán, *J. Phys. Chem. Lett.*, 2015, **6**, 4270–4279.
- 9 J. H. Espenson, *Chemical Kinetics and Reaction Mechanisms*, McGraw-Hill, 1995.
- 10 Q. Liu, W. Jia and F. Li, *Sci. Rep.*, 2020, **10**, 11664.
- 11 S. Pahl, miopython (version v2.3.2) Zenodo 2023.
- 12 P. B. Johnson and R. W. Christy, *Phys. Rev. B*, 1972, **6**, 4370–4379.
- 13 K. Metwally, S. Mensah and G. Baffou, *J. Phys. Chem. C*, 2015, **119**, 28586–28596.
- 14 M. Alrahili, V. Savchuk, K. McNear and A. Pinchuk, *Sci. Rep.*, 2020, **10**, 18790.
- 15 G. Baffou, R. Quidant and F. J. García de Abajo, *ACS Nano*, 2010, **4**, 709–716.
- 16 A. O. Govorov, W. Zhang, T. Skeini, H. Richardson, J. Lee and N. A. Kotov, *Nanoscale Res. Lett.*, 2006, **1**, 84.
- 17 M. Chen, Y. He, Y. Hu and J. Zhu, *Plasmonics*, 2019, **14**, 1893–1902.